

Earth's Future

RESEARCH ARTICLE

10.1029/2023EF003788

Yunhua Mo and Shouzhi Chen contributed equally to this work.

Key Points:

- Process-based models outperform statistical models in forecasting changes in spring vegetation phenology in the Northern Hemisphere
- Simulated start of the growing season explained >75% of the percentage of variance
- Trend of advance in the start of the growing season in the Northern Hemisphere will reverse by 2060 under moderate warming conditions

Supporting Information:

Supporting Information may be found in the online version of this article.

Correspondence to:

Y. Fu,
yfu@bnu.edu.cn

Citation:

Mo, Y., Chen, S., Wu, Z., Tang, J., & Fu, Y. (2024). The advancement in spring vegetation phenology in the Northern Hemisphere will reverse after 2060 under future moderate warming scenarios. *Earth's Future*, 12, e2023EF003788. <https://doi.org/10.1029/2023EF003788>

Received 11 MAY 2023


Accepted 13 FEB 2024

Author Contributions:

Conceptualization: Yongshuo Fu
Data curation: Yunhua Mo
Formal analysis: Yunhua Mo
Funding acquisition: Yongshuo Fu
Investigation: Jing Tang, Yongshuo Fu
Methodology: Yunhua Mo, Yongshuo Fu
Software: Yunhua Mo
Supervision: Jing Tang, Yongshuo Fu
Validation: Yunhua Mo
Visualization: Yunhua Mo

© 2024 The Authors. *Earth's Future* published by Wiley Periodicals LLC on behalf of American Geophysical Union. This is an open access article under the terms of the [Creative Commons Attribution-NonCommercial-NoDerivs License](#), which permits use and distribution in any medium, provided the original work is properly cited, the use is non-commercial and no modifications or adaptations are made.

The Advancement in Spring Vegetation Phenology in the Northern Hemisphere Will Reverse After 2060 Under Future Moderate Warming Scenarios

Yunhua Mo¹, Shouzhi Chen¹ , Zhaofei Wu¹, Jing Tang^{2,3}, and Yongshuo Fu^{1,4} 

¹College of Water Sciences, Beijing Normal University, Beijing, China, ²Department of Physical Geography and Ecosystem Science, Lund University, Lund, Sweden, ³Terrestrial Ecology Section, Department of Biology, University of Copenhagen, Copenhagen, Denmark, ⁴Plants and Ecosystems, Department of Biology, University of Antwerp, Wilrijk, Belgium

Abstract Global warming has largely advanced spring vegetation phenology, which has subsequently affected terrestrial carbon and water cycles. However, further shifts in vegetation phenology under future climate change remain unclear. We estimated the start of the growing season (SOS) by applying multiple extraction methods based on the NDVI3g data set, and then parameterized and evaluated 11 spring vegetation phenology models that included chilling, forcing, and the photoperiod. Based on scenario data from three Shared Socioeconomic Pathways (SSP126, SSP245, and SSP585) derived from eight climate models, future vegetation phenology was predicted using the phenology models. Results showed that all the phenology models performed better than the NULL model (mean of the SOS), with the performance of one-phase models broadly matching that of two-phase models, although the best models varied by vegetation type. The spatial pattern of simulated SOS was similar among the models, and it explained >75% of the variation. Based on the mean predicted SOS, we found that spring vegetation phenology will continue to advance under strong warming conditions (SSP245 and SSP585), but that the trend of advance will reverse at around 2060 under the SSP126 scenario. The continued trend in SOS advance is likely related to rapid forcing fulfillment under stronger warming conditions. However, under moderate warming, chilling might be reduced and it might require longer to compensate for higher forcing, which ultimately would result in SOS delay. Our findings highlight that trends will likely change under different warming conditions, potentially causing widespread impact on species interaction, biodiversity, and ecosystem function.

Plain Language Summary Phenological change, which is often seen as an indicator of climate change, has received widespread attention. However, despite this focus, comprehension of how vegetation phenology might alter under different climate change scenarios remains inadequate. We used 11 process-based phenology models to forecast changes in the start of the growing season (SOS) in the Northern Hemisphere under 3 climate change scenarios (SSP126, SSP245, and SSP585). Results showed that the one-phase models and the two-phase models exhibited similar performance, which exceeded that of the NULL model (mean of the SOS). Under the strong warming scenarios (SSP245 and SSP585), spring phenology was projected to continue to advance, whereas under the moderate warming scenario (SSP126), the trend of advance was predicted to reverse at around 2060. Our findings suggest that climate change might alter the competition between species for spring resources, and thereby have widespread impact both on biodiversity and on the structure and function of ecosystems.

1. Introduction

Evidence for recent warming of Earth's climatic system is incontrovertible (Solomon, 2007). During 1880–2012, the mean surface temperature of Earth increased by 0.85°C (Stocker, 2014). Compared with 1850–1900, the 20-year mean global surface temperature rose by 0.99°C during 2001–2020, whereas the 10-year mean global surface temperature increased by approximately 1.09°C during 2011–2020 (Masson-Delmotte et al., 2021), implying that surface warming is ongoing. Changes in the climatic system broadly affect every region on Earth, and the role of human activities in the recent warming of the atmosphere, oceans, and land has been identified (Masson-Delmotte et al., 2021). Because some changes in the climatic system of Earth are irreversible, it is critical to assess the impact of future climate change on terrestrial ecosystems.

Writing – original draft: Yunhua Mo, Yongshuo Fu
Writing – review & editing: Yunhua Mo, Shouzhi Chen, Zhaofei Wu

Vegetation phenology is a key indicator of climate change (Fu et al., 2019; Jeong et al., 2011), and obtaining phenological metrics is the underlying premise of the study of climate change through phenology. The methods used to obtain vegetation phenology can be divided into three categories: ground-based phenology observations, remote-sensing-based phenology observations, and phenology modeling. Ground-based phenology observations often rely on volunteer observations of the phenological period of natural and cultivated species (Cleland et al., 2007). As a traditional and widely used method, it can accurately and continuously describe the phenological status of specific plant species (Piao et al., 2019). Although ground-based phenology observations can be used as reference, they are constrained by the limited number of observed plant species, limited distribution range, and level of observational skill (Menzel, 2002; Piao et al., 2019).

In recent decades, with the development of remote sensing technology, phenology observations based on remote sensing have received increasing attention (Berra & Gaulton, 2021). The vegetation phenology obtained using remote sensing techniques is usually based on time series of vegetation indexes such as the normalized difference vegetation index (NDVI), enhanced vegetation index, and Sun-induced chlorophyll fluorescence calculated from the reflectance of the vegetation canopy (Chen et al., 2021; F. Meng et al., 2021; L. Meng et al., 2021; Reed et al., 2009). Although remote sensing has advantages in large-scale phenological research, it is limited by problems such as mixed pixels (Zeng et al., 2020). Neither ground-based phenology observations nor remote-sensing-based phenology observations can predict future phenology. In contrast, the phenology modeling approach is based on the impact of environmental factors on vegetation phenology and therefore it can be used for phenological prediction.

Vegetation phenology is driven by abiotic and biotic factors (Lieth, 1974; Pau et al., 2011; Wolkovich et al., 2014). Biotic factors include competition between plant species (Morales et al., 2005), while abiotic factors include CO₂ concentration, climate change, nitrogen deposition, and land use change (Piao et al., 2020). Environmental factors that affect vegetation phenology include the temperature, photoperiod, and precipitation (Fu et al., 2020). The manifestation of spring vegetation phenology is closely associated with dormancy, which encompasses three distinct phases: paradormancy, endodormancy, and ecodormancy (Lang et al., 1987). In phenological modeling, a model that explains only ecodormancy (forcing) is called a one-phase model, whereas a model that explains both endodormancy and ecodormancy (chilling and forcing) is called a two-phase model. The earliest one-phase model based on environmental factors was introduced by Reaumur (1735). The model, which considers only the effect of temperature and uses accumulated heat to measure phenological progress, is known as the “thermal time” model (Basler, 2016). Subsequently, with consideration of new explanations for dormancy, many more one-phase and two-phase models were gradually developed. Accounting for the temperature response function (linear and sigmoid) and environmental driving factors (temperature and photoperiod), one-phase models include the TT, TTs, M1, and M1s thermal time models, and the PTT and PTTs photothermal time models (Chuine et al., 1999; Hunter & Lechowicz, 1992; Wang, 1960). Based on the order of onset of the chilling process and the forcing process, two-phase models can be classified as sequential, parallel, and alternate models (Cannell & Smith, 1983; Hänninen, 1990; Kramer, 1994; Murray et al., 1989).

Spring vegetation phenology regulates the photosynthesis of the canopy and subsequent terrestrial ecosystem processes, thereby affecting biosphere–atmosphere interaction (Piao et al., 2019), which also affects interspecific competition and the structure and function of ecosystems (Huang et al., 2017). The continuous advance of spring vegetation phenology has had huge impact on the carbon sink of terrestrial ecosystems (Keenan et al., 2014). Consequently, large-scale phenological monitoring is important for understanding the carbon cycling processes of terrestrial ecosystems. Phenology models are often established at the site scale and used for prediction of the spring phenology for specific tree species; thus, large-scale phenological simulations are relatively rare. Therefore, there is urgent need to evaluate large-scale spring vegetation phenology forecasts under different climate change scenarios, especially the latest Shared Socioeconomic Pathway (SSP) scenarios, owing to the great importance for future management and protection of terrestrial ecosystems.

In this study, 11 spring phenology models were parameterized by combining the start of the growing season (SOS) derived from remote sensing and meteorological data from the historical period (1982–2015). The spring phenological models included six one-phase models and five two-phase models. Then, predictions of future spring vegetation phenology for 2016–2100 were produced using data from three SSP scenarios. The objectives of this study were (a) to compare the performance of different spring vegetation phenology models, and (b) to

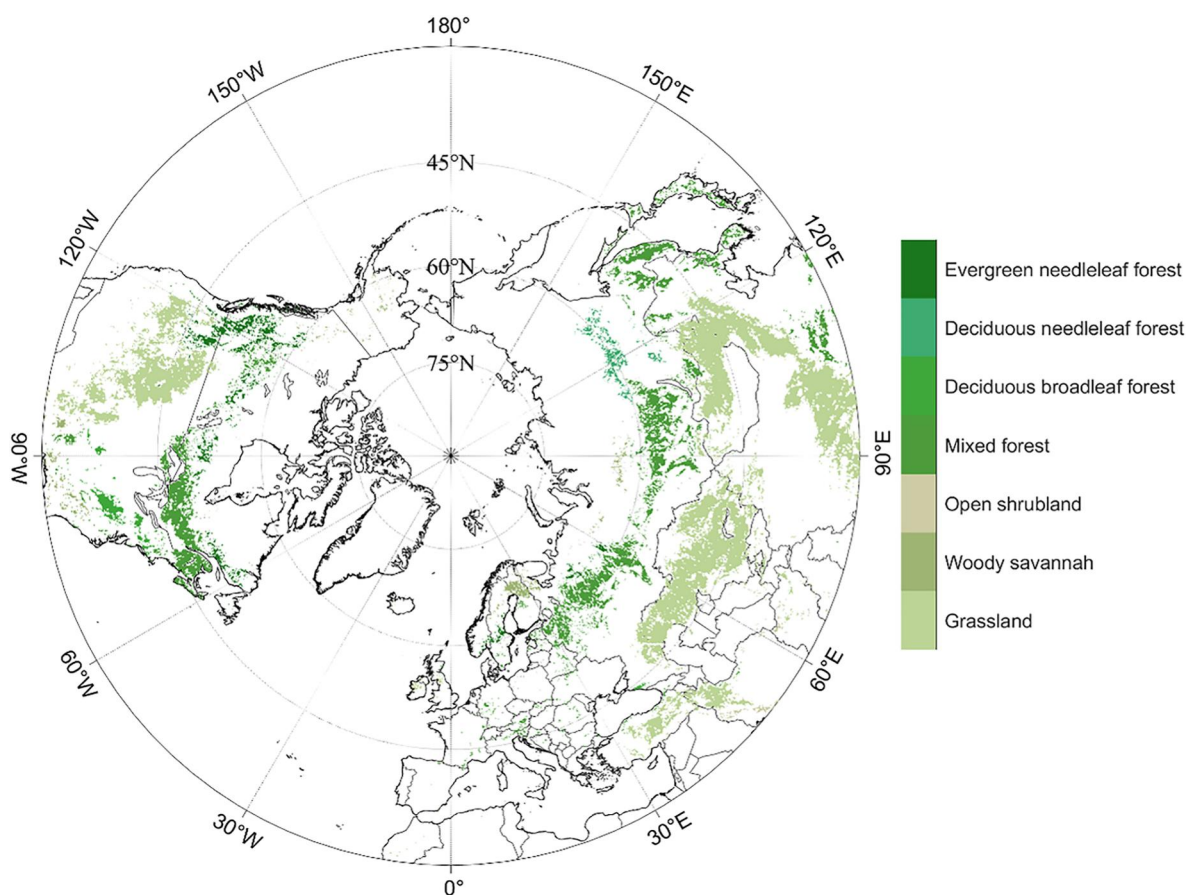


Figure 1. Distribution of the considered vegetation types within the study area.

evaluate the changes in spring phenology and reveal whether spring phenology will continue to advance in the future under different warming scenarios.

2. Materials and Methods

2.1. Study Region and Vegetation Type

The study region comprised the Northern Hemisphere above 30°N. The vegetation map we used was obtained by aggregation of the Moderate Resolution Imaging Spectroradiometer standard land cover data product (MCD12C1) with spatial resolution of 1/12° (Figure 1). The International Geosphere–Biosphere Program (IGBP) classification system was used to reclassify the pixels, and we adopted the following criteria: (a) exclusion of crop-dominated areas because cropland is susceptible to disturbance by human activity, and (b) selection of pure pixels of each vegetation type that have not changed during 2000–2020 (the fraction of a given vegetation type is equal to 100). Ultimately, seven vegetation types were obtained: evergreen needleleaf forest (ENF), deciduous needleleaf forest (DNF), deciduous broadleaf forest (DBF), mixed forest (MF), open shrubland (OSL), woody savannas (WS), and grassland (GL).

2.2. NDVI and Phenological Extraction

Retrieval of phenological information is prerequisite for parametric phenology models. In this study, the Advanced Very High Resolution Radiometer Global Inventory Modeling and Mapping Studies third-generation 15-day composite NDVI product (NDVI3g) was used to extract vegetation spring phenology, because it is widely used for extraction of phenological metrics (Mo et al., 2019; Piao et al., 2006). The data set spans 1982–2015 and has spatial resolution of 1/12°. It eliminates effects such as orbital drift and sensor calibration, and undergoes quality control with higher resolution data (Pinzon & Tucker, 2014).

Extraction of vegetation phenology based on the NDVI typically involves two steps: fitting the NDVI curve and determining the phenological metrics. Considering the uncertainty in using a single method (White et al., 2009), five methods were used to retrieve the SOS data. The NDVI curve fitting methods used in this study were Gaussian, Spline, Harmonic Analysis of Time Series, Polyfit, and the Savitzky–Golay filter (Jakubauskas et al., 2001; Jonsson & Eklundh, 2002; Jönsson & Eklundh, 2004; Piao et al., 2006; Roerink et al., 2000; White et al., 2009; Wu et al., 2010; Yu et al., 2010). The methods adopted for determination of the phenological period included the dynamic threshold method and the maximum change rate method based on the fitting of the NDVI curve. The dynamic threshold method takes the date when the NDVI value reaches a specific ratio between the minimum NDVI and the maximum NDVI of the year as the SOS, and commonly used ratios are 20% and 50%. The maximum change rate method takes the date with the maximum rate of change of the fitted NDVI curve as the SOS. In this study, the Gaussian and Spline methods used the 50% dynamic threshold method for determination of the phenological period, the Harmonic Analysis of Time Series and Polyfit methods used the maximum change rate method, and the Savitzky–Golay filter used the 20% dynamic threshold method (Cong et al., 2013). The curve fitting functions for the five methods and the method adopted for determination of the SOS are summarized in Table S1 in Supporting Information S1. We used the mean of the five methods as input data to parameterize the 11 models (Figure 2I).

2.3. Meteorological Data

2.3.1. Historical Climate Data Set

The historical climate data used for model parameterization were extracted from the ERA-Interim data set. ERA-Interim is a new generation of reanalysis products following ERA-40 that incorporates new technologies to improve data quality. The ERA-Interim data set offers global atmospheric reanalysis data extending from 1 January 1979–31 August 2019 at various spatial resolutions from 0.125° to 2.5° (Berrisford et al., 2009, 2011). We downloaded daily atmospheric temperature data from 1982 to 2015 at 2-m height above the ground with 0.125° spatial resolution. The average of the temperature at four instances (06, 12, 18, and 24 hr) was calculated as the daily mean temperature.

2.3.2. Climate Scenario Data Set

The international Coupled Model Intercomparison Project Phase 6 (CMIP6) of the World Climate Research Program developed a new set of scenarios run in the 21st century that represent different degrees of socioeconomic development and different pathways for change in atmospheric greenhouse gas concentrations (Eyring et al., 2016; Li et al., 2021; O'Neill et al., 2016). The five main SSP scenarios are SSP1-1.9, SSP1-2.6, SSP2-4.5, SSP3-7.0, and SSP5-8.5, where the first number represents the SSP and the second number represents the radiative forcing level by 2100. For example, the SSP1-2.6 scenario represents an approximate total radiative forcing level of 2.6 W m⁻² by 2100 under the SSP1 socioeconomic pathway, which broadly corresponds to Representative Concentration Pathway (RCP) 2.6 used in the previous generation of climate change scenarios (Meinshausen et al., 2020). This study selected three SSP scenarios: SSP1-2.6 (SSP126), SSP2-4.5 (SSP245), and SSP5-8.5 (SSP585). Considering the uncertainty associated with individual climate models, we estimated the phenology using eight CMIP6 climate models (i.e., BCC-CSM2-MR, INM-CM4-8, INM-CM5-0, MIROC6, MPI-ESM1-2-LR, MRI-ESM2-0, NorESM2-LM, and NorESM2-MM) and computed their average as the projected future spring vegetation phenology. Information regarding the global climate models employed in this study is summarized in Table S2 in Supporting Information S1.

2.4. Spring Vegetation Phenology Models

Spring phenology in the study area is controlled mainly by temperature and the photoperiod. We selected 11 spring vegetation phenology models for use in this study, of which 3 models considered only the influence of temperature and 8 models considered the influence of both temperature and photoperiod (Table 1). From the perspective of dormant release, six one-phase models and five two-phase models were used, which included between three and eight parameters. Tables S3 and S4 in Supporting Information S1 summarize the functions used by the 11 models and provide descriptions of the parameters.

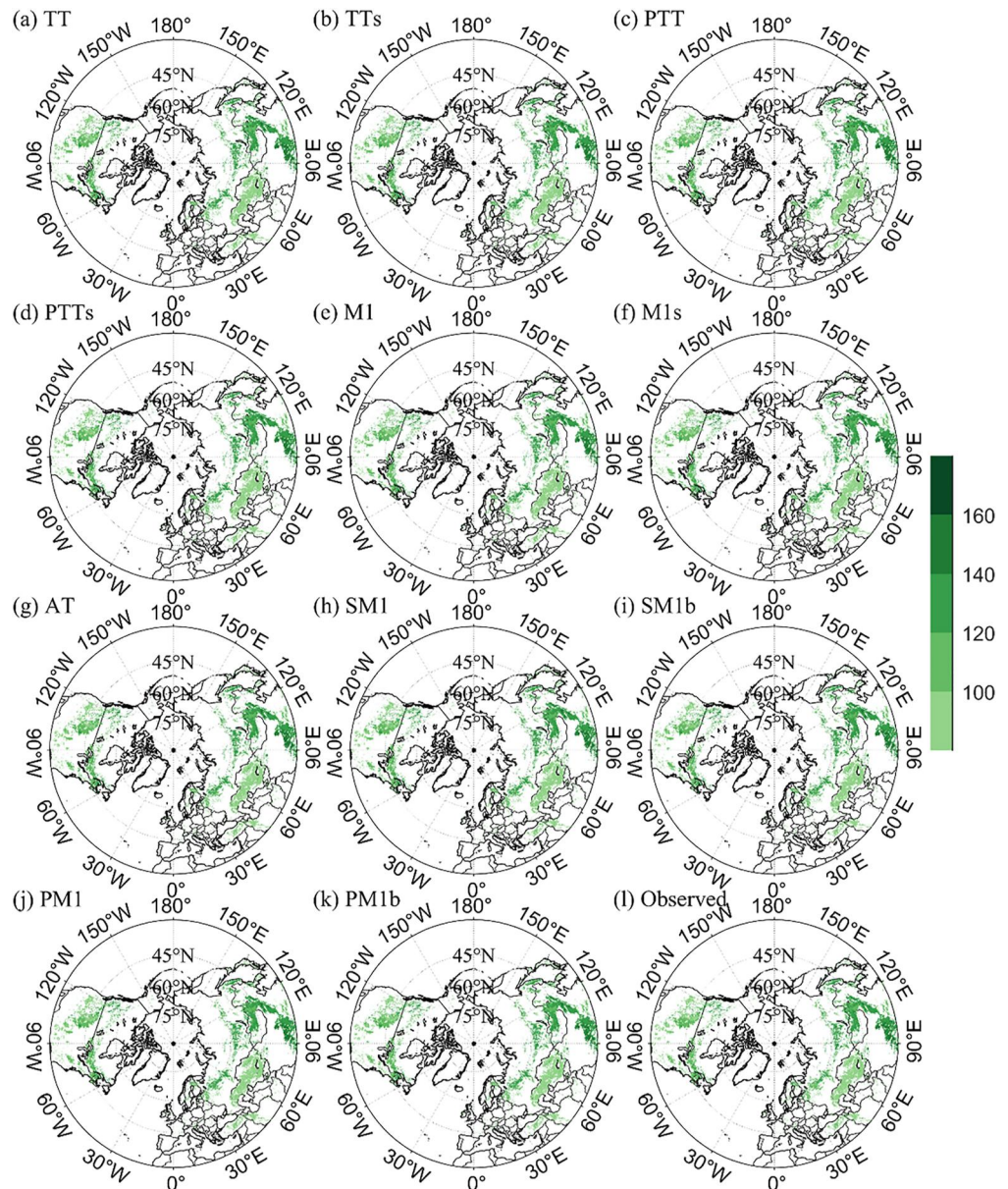


Figure 2. Spatial pattern of the multiyear mean start of the growing season (SOS) (a–k) predicted by each of the 11 spring phenology models and (l) observed by satellite.

2.5. Model Calibration

To improve model robustness, we used the SOS for each pixel for 26 years (i.e., 1986–2011) to parameterize the spring phenology model, and we used that for another 8 years (i.e., 1982–1985 and 2012–2015) to evaluate model performance. Our modeling study was based on the PHENOR phenology modeling framework (Hufkens et al., 2018), and the model parameterization method was based on the generalized simulated annealing package (Xiang et al., 2013).

We used the correlation coefficient (r), root mean square error (RMSE), and Akaike information criterion (AIC) to evaluate model performance. The RMSE is often used to measure the difference between the predicted and observed values of a model. The smaller the RMSE value, the closer the predicted and observed values. The RMSE is calculated using the following formula:

Table 1
Spring Vegetation Phenology Models Used in This Study

Model abbreviation	Full model name	Release	Drivers	Structure	No. parameters	Comments/References
NULL	NULL model					Mean of the SOS (Table S3 in Supporting Information S1)
TT	Thermal Time model	Ecodormancy release	F	One-phase	3	Chuine et al. (1999), Kramer (1994), and Reaumur (1735)
TTs	Thermal Time model	Ecodormancy release	F	One-phase	4	Hänninen (1990) and Kramer (1994)
PTT	Photothermal Time model	Ecodormancy release	PF	One-phase	3	Masle et al. (1989)
PTTs	Photothermal Time model	Ecodormancy release	PF	One-phase	4	Basler (2016), Landsberg (1974), and Črepinšek et al. (2006)
M1	M1 model	Ecodormancy release	PF	One-phase	4	Blümel and Chmielewski (2011)
M1s	M1 model	Ecodormancy release	PF	One-phase	5	M1 model using a sigmoid temperature response
AT	Alternating model	Endo- and ecodormancy releases	CF	Two-phase	5	Murray et al. (1989)
SM1	Sequential model (M1 variant)	Endo- and ecodormancy releases	CFP	Two-phase	8	Basler (2016)
SM1b	Sequential model (M1 variant)	Endo- and ecodormancy releases	CFP	Two-phase	8	SM1 model using a bell-shaped chilling response
PM1	Parallel M1 model	Endo- and ecodormancy releases	CFP	Two-phase	8	Basler (2016)
PM1b	Parallel M1 model	Endo- and ecodormancy releases	CFP	Two-phase	8	PM1 model using a bell-shaped chilling response

Note. Model description: SOS: start of the growing season; s: using a sigmoid temperature response for forcing rather than a growing-degree-day temperature response; b: using a bell-shaped temperature response for chilling rather than a triangular temperature response. Driver abbreviations: C: chilling temperature, F: forcing temperature, and P: photoperiod. Combinations of different letters in the driver column represent those drivers that are driving the model.

$$RMSE = \sqrt{\frac{\sum_{i=1}^n (OBS_i - PRE_i)^2}{n}} \quad (1)$$

where OBS_i is the i th observation, PRE_i is the i th predicted value, and n is the number of observations.

The AIC, which accounts for both the model complexity and the goodness-of-fit to the data, is widely employed for model selection. A smaller AIC value indicates better model performance. The AIC is calculated as follows:

$$AIC = n \cdot \log(RMSE^2) + 2k + \frac{2k(k+1)}{n-k-1} \quad (2)$$

where k is the number of parameters included in the model.

3. Results

3.1. Model Validation and Performance Comparison

We used satellite-derived SOS and ERA-Interim meteorological data to parameterize and validate the phenology models for the seven types of vegetation in spring in the Northern Hemisphere. The simulation of SOS by each of the 11 models (Figures 2a–2k) produced a similar spatial pattern to that of the satellite-derived SOS (Figure 2l). Overall, the SOS was progressively delayed with increasing latitude. However, the mean and the standard deviation of the SOS varied depending on vegetation type (Figure S1 in Supporting Information S1). Specifically, OSL had the earliest SOS, averaging approximately 90 days, whereas ENF had the latest SOS, which was approximately 30 days later than that of OSL. DNF had the smallest standard deviation of SOS at approximately 5.6 days, followed by that of DBF at approximately 9.5 days; GL had the largest standard deviation of SOS at over 22 days. These

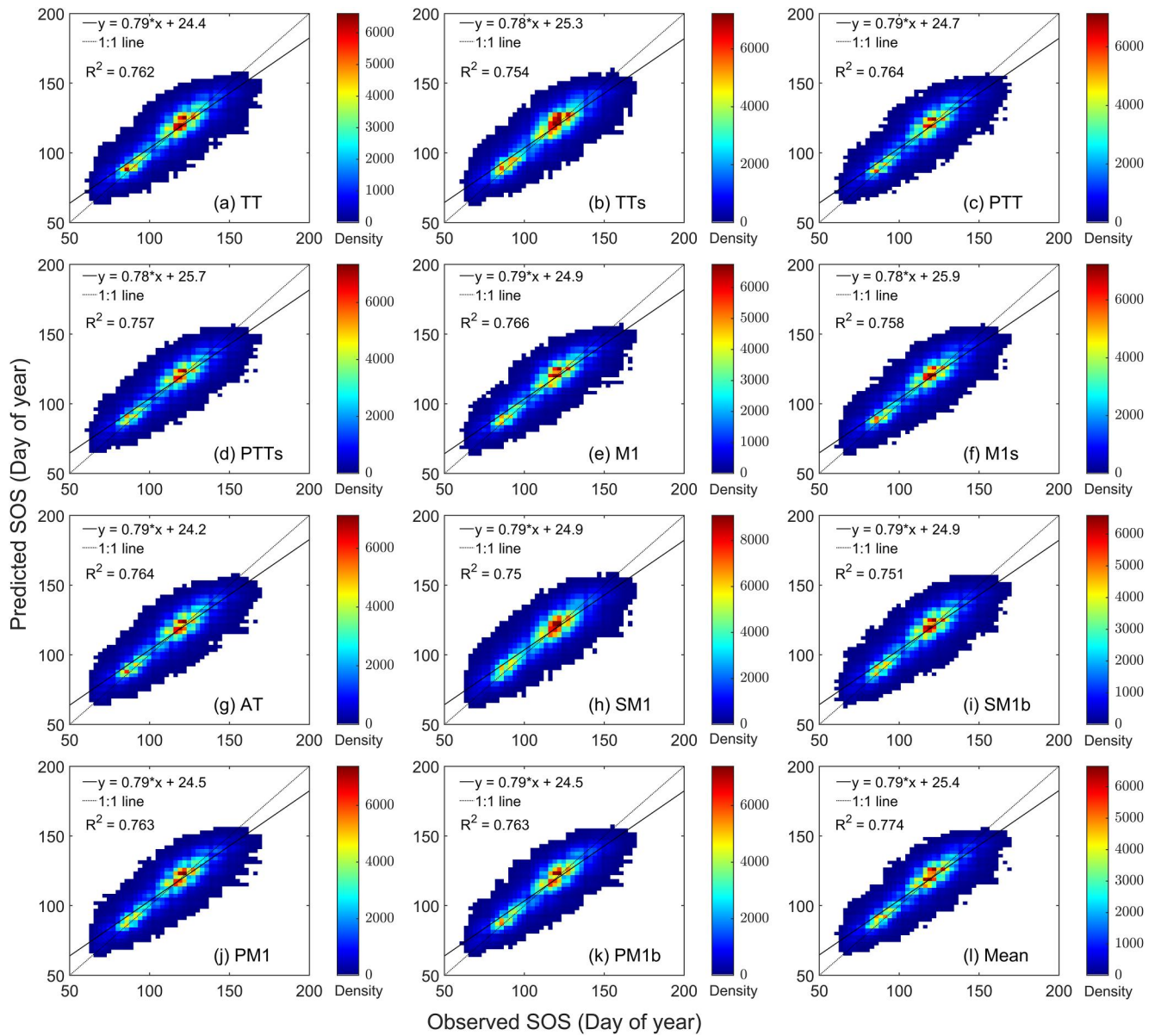


Figure 3. Heat plots of model-predicted and satellite-derived SOS: (a–k) for each of the 11 spring phenology models and (l) for the mean predicted SOS of all 11 models.

results suggest that the SOS of woody plants is relatively concentrated, whereas that of herbaceous plants spans a longer period.

Overall, the percentage of variance explained by the 11 models ranged from 75% (SM1) to 76.6% (M1), with slope of 0.78–0.79 for the linear fits (Figure 3). For all vegetation types, the RMSEs of the 11 models were smaller than those of the NULL model (Table 2). For all models, the RMSE was within 15 days for most pixels; however, there were large differences between the results for different vegetation types (Figure S2 in Supporting Information S1). Specifically, DNF had the smallest RSME, averaging approximately 5.2 days, whereas ENF had the largest RMSE, averaging 13.2 days (Table 2, Figure S1 in Supporting Information S1). For WS and GL, the model-simulated SOS had the highest correlation coefficient with the satellite-derived SOS, both averaging 0.9, whereas the correlation coefficient was smallest for DNF, averaging 0.6.

Overall, the one-phase models demonstrated performance comparable to that of the two-phase models; however, it varied depending on vegetation type (Table 2). The two-phase models exhibited slightly better performance than the one-phase models for DBF and MF, whereas the one-phase models demonstrated slightly better

Table 2
Summary of the Comparison Between the Satellite-Derived Start of Growing Season (SOS) and Simulated SOS of the 11 Models for the 7 Vegetation Types: Evergreen Needleleaf Forest (ENF), Deciduous Needleleaf Forest (DNF), Deciduous Broadleaf Forest (DBF), Mixed Forest (MF), Open Shrubland (OSL), Woody Savannah (WS), and Grassland (GL)

Vegetation type	NULL	TT	TTS	PTT	PTTs	MI	MIs	AT	SMI	SMIb	PMI	PMIb
ENF	RMSE (days)	13.0	13.3	13.0	13.2	13.0	13.3	12.9	13.5	13.4	13.1	13.0
	<i>r</i>	-	0.72 ^a	0.71 ^a	0.71 ^a	0.70 ^a	0.70 ^a	0.72 ^a	0.69 ^a	0.70 ^a	0.71 ^a	0.72 ^a
	AIC	-	189,007	190,669	189,117	190,315	189,225	190,578	188,333	191,760	189,350	189,276
DNF	RMSE (days)	5.6	5.3	5.1	5.3	5.2	5.0	5.4	5.4	5.3	5.3	5.3
	<i>r</i>	-	0.60 ^a	0.60 ^a	0.60 ^a	0.61 ^a	0.62 ^a	0.60 ^a	0.60 ^a	0.60 ^a	0.60 ^a	0.60 ^a
	AIC	-	47,358	46,317	47,428	45,919	46,605	45,621	47,821	47,444	47,122	47,103
DBF	RMSE (days)	9.5	7.8	8.3	7.6	7.5	8.0	7.7	7.7	7.8	7.7	7.7
	<i>r</i>	-	0.64 ^a	0.57 ^a	0.65 ^a	0.57 ^a	0.66 ^a	0.66 ^a	0.64 ^a	0.63 ^a	0.65 ^a	0.65 ^a
	AIC	-	34,232	35,214	33,919	35,178	33,620	34,652	34,021	34,049	34,078	34,113
MF	RMSE (days)	13.7	9.5	9.8	9.4	9.3	9.7	9.4	9.7	9.7	9.4	9.4
	<i>r</i>	-	0.73 ^a	0.71 ^a	0.73 ^a	0.71 ^a	0.73 ^a	0.73 ^a	0.71 ^a	0.71 ^a	0.73 ^a	0.73 ^a
	AIC	-	796,547	807,698	794,130	805,533	791,013	805,242	795,605	804,949	795,227	794,971
OSL	RMSE (days)	15.7	9.3	9.4	9.3	9.1	9.3	9.3	9.7	9.6	9.2	9.2
	<i>r</i>	-	0.82 ^a	0.81 ^a	0.82 ^a	0.81 ^a	0.82 ^a	0.81 ^a	0.80 ^a	0.81 ^a	0.82 ^a	0.82 ^a
	AIC	-	14,489	14,580	14,484	14,602	14,345	14,517	14,498	14,761	14,402	14,422
WS	RMSE (days)	15.4	6.9	6.8	6.9	6.5	6.6	7.0	7.2	7.1	6.7	6.7
	<i>r</i>	-	0.90 ^a	0.90 ^a	0.90 ^a	0.90 ^a	0.91 ^a	0.90 ^a	0.89 ^a	0.89 ^a	0.91 ^a	0.90 ^a
	AIC	-	68,537	68,205	68,442	67,710	66,221	66,968	68,970	70,027	67,246	67,440
GL	RMSE (days)	22.5	9.8	9.8	9.7	9.7	9.8	9.7	10.0	10.0	9.7	9.7
	<i>r</i>	-	0.90 ^a	0.90 ^a	0.90 ^a	0.90 ^a	0.90 ^a	0.90 ^a	0.90 ^a	0.90 ^a	0.90 ^a	0.90 ^a
	AIC	-	1,326,157	1,330,531	1,324,130	1,327,758	1,321,933	1,325,409	1,324,528	1,340,312	1,324,938	1,325,256

Note. The model abbreviations are as listed in Table 1, and model performance was evaluated using the metrics of the root mean square error (RMSE), correlation coefficient (*r*), and Akaike information criterion (AIC). ^aStatistical significance at *p* < 0.001.

performance than the two-phase models for the remaining vegetation types. We used the AIC to identify the best model for each vegetation type. Results showed that ENF was best represented by the AT model, while the M1s model performed best for DNF, and the M1 model showed best performance for the remaining five vegetation types.

The RMSE does not reflect the relative magnitude between the model simulations and the satellite observations; therefore, we calculated the difference between the average model-simulated SOS and the satellite-derived SOS for 1982–2015. Overall, the errors in the model-simulated SOS had similar spatial distribution (Figure 4). The mean error was <6 days for most pixels, and there was no clear pattern of distribution in the latitudinal direction. However, the distribution of errors varied considerably between vegetation types. Specifically, the model-simulated SOS for WS was smaller than that observed by satellite for most pixels, whereas the model-simulated SOS was generally larger than that observed by satellite for the other vegetation types.

3.2. Temperature-Change-Induced Variation in Chilling Days

To evaluate how chilling days might vary under the different scenarios, we first calculated the change in mean temperature over 2016–2100 under three SSP scenarios in the regions where the seven vegetation types are located (Figure S3 in Supporting Information S1). Regions containing OSL exhibited the highest mean annual temperature, whereas areas containing DNF had the lowest mean annual temperature. Temperature variations were notably distinct across the three scenarios, particularly post-2060. Under the SSP126 scenario, temperatures initially exhibited a trend of increase followed by gradual decline; however, by 2100, the average temperature remained higher than that of 2016. Under the SSP245 scenario, the rate of increase in temperature diminished after 2060, resulting in overall warming of over 2°C during 2016–2100. Under the SSP585 scenario, average temperatures across all vegetation types demonstrated a consistent and progressive increase, with the average rise exceeding 5°C in 2100 relative to 2016.

To reflect the differences in the change in average temperature over different periods and under the different scenarios, we calculated the difference between the average temperature of four periods, that is, 2021–2040, 2041–2060, 2061–2080, and 2081–2100, and the average temperature of the historical period, that is, 1982–2015 (Figure S4 in Supporting Information S1). Under all three scenarios, the average temperature of regions of WS during 2021–2040 was lower than that of the historical period. Under scenario SSP126, the magnitude of the temperature increase gradually increased from 2021 to 2040 to 2061–2080 and then it dropped to the 2041–2060 level during 2081–2100, although there were differences in the temperature changes among the different vegetation types. Under the SSP245 and SSP585 scenarios, the magnitude of the temperature increase gradually increased from 2021–2040 to 2081–2100, with the average temperature of regions of WS changing from a value below the historical level to a value above the historical level.

With change in temperature, especially warming, the effect of chilling might be impacted. We employed the concept of chill days to evaluate the fulfillment of chilling requirements, which is characterized by the accumulation of the number of days within a specific temperature range. In this study, chill days were defined as the number of days with a temperature of 0–10°C between 1 September of the previous year and the average SOS (Figures 5 and 6). On average, the number of chill days gradually increased under the warming scenarios, and the trend of increase under moderate warming conditions shifted at around 2060 (Figure 5h). Specifically, under the various warming scenarios, the number of chill days gradually increased (decreased) for ENF, DNF, MF, WS, and GL (DBF and OSL). Under the moderate warming scenarios, the trend of chill days shifted at around approximately 2060. Compared with that under the SSP126 and SSP245 scenarios, pronounced increase in the spatial extent of chill days was evident under the SSP585 scenario, which would be expected to result in reduction in the temperature accumulation required for the spring plant forcing process, thereby leading to SOS advancement (Figure 6).

3.3. Future Spring Phenological Changes

Under the different warming scenarios, the phenological changes of the different vegetation types vary (Figure 7). On average, during 2016–2060, the SOS had a similar trend under both the SSP126 and the SSP245 scenarios. After 2060, the SOS under the SSP245 scenario tended to advance gradually, whereas it was gradually delayed under the SSP126 scenario. Under the SSP585 scenario, the SOS advanced gradually during 2016–2100 at a rate of approximately 0.12 days per year (Figure 7h). Under the SSP126 scenario, the SOS for the various vegetation types exhibited initial advancement followed by subsequent delay, except for OSL. Under the SSP245 scenario,

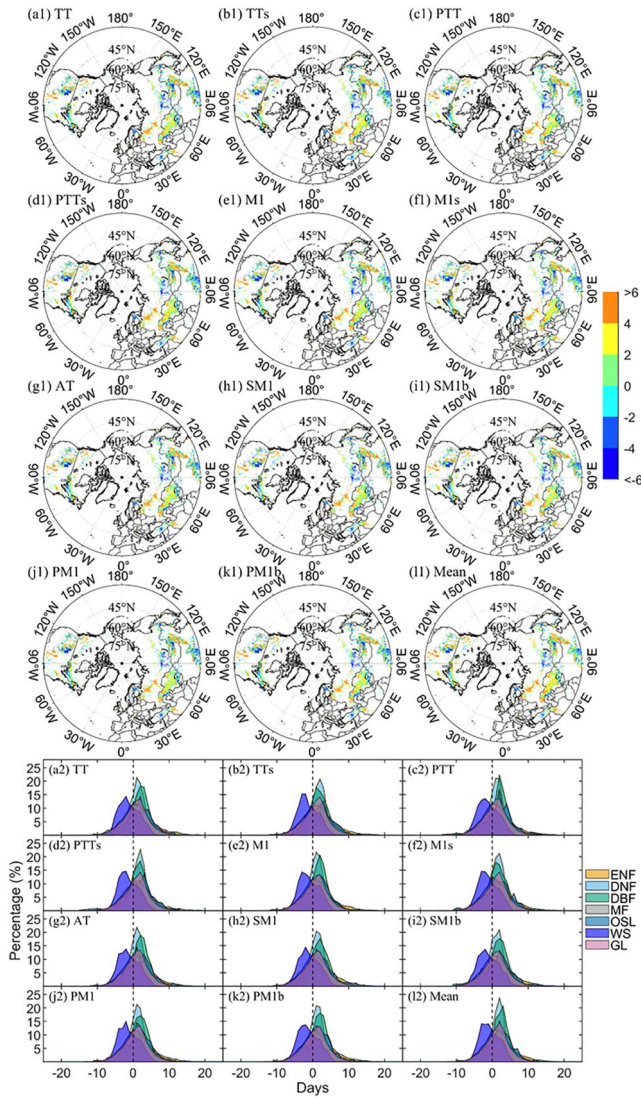


Figure 4. Spatial distribution and histogram of the mean error of the model simulation results for the seven vegetation types. (a1–l1) Spatial distributions of the average errors of the simulation results of the 11 spring phenology models and their mean, and (a2–l2) error histograms of the SOS of the seven vegetation types simulated by the 11 models and their mean. The seven vegetation types comprise evergreen needleleaf forest (ENF), deciduous needleleaf forest (DNF), deciduous broadleaf forest (DBF), mixed forest (MF), open shrubland (OSL), woody savannah (WS), and grassland (GL).

the SOS experienced gradual advancement, and the rate of progression diminished to varying extents post-2060. The SOS of all seven vegetation types under the SSP585 scenario showed a trend of gradual advance, with that of ENF having the highest rate of advancement (approximately 0.21 days per year), and that of OSL and GL having the smallest rate of advancement (approximately 0.07 days per year).

To capture the average phenological changes across different periods and under different scenarios, we computed the differences between the mean SOS of the four periods (2021–2040, 2041–2060, 2061–2080, and 2081–2100) and the mean SOS of the historical period (1982–2015), as shown in Figure 8. Generally, the changes in SOS were similar under the SSP126 and SSP245 scenarios, with differences mainly occurring after 2060. Specifically, the SOS of DNF and WS was later than the average of 1982–2015, whereas the SOS of the other vegetation types was earlier. Under the SSP585 scenario, the SOS generally became earlier, with the SOS of WS gradually shifting from being later than the historical average to being earlier than the historical average. Although the SOS of DNF remained later than the average of 1982–2015, the magnitude of the difference gradually decreased.

4. Discussion

4.1. Model Performance

Our results showed that the predictions of all 11 models were generally close, although the models demonstrating the best performance varied with vegetation type. Previous studies that compared models, conducted at both the site scale and the large scale (based on remote sensing), yielded similar results. This variation might arise owing to differences in the mechanisms driving phenological development across distinct regions or vegetation types. Currently, phenological modeling research lacks a unified model capable of comprehensively simulating all scenarios. For example, Vitasse et al. (2011) tested phenology models using phenological observations of six European tree species compiled over 2–3 years and found that for most species, one-phase models demonstrated comparable performance to that of two-phase models. Basler (2016) tested existing phenology models and their combinations using long-term phenological observations from Central Europe and found that one-phase models had similar or better performance than two-phase models. Zhao et al. (2021) compared four existing models using European phenological observations and found that two-phase models performed slightly better than the one-phase model. In terms of large-scale model comparison, Liu et al. (2018) compared the performance of one-phase and two-phase models using satellite-based Northern Hemisphere phenology and found that the best-performing model varied by vegetation type. Our recent large-scale model comparison study demonstrated that one-phase and two-phase models yield comparable results (Mo, Zhang, Jiang, et al., 2023; Mo, Zhang, Liu, et al., 2023). It should be noted that Liu et al. (2018) and Zhao et al. (2021) both used only a single one-phase model in their studies, which might have introduced some degree of uncertainty in their results. To enhance the accuracy of vegetation phenology simulation, improvements could be pursued on two fronts: augmentation of the mechanistic aspects of models to enhance their ability to simulate complex scenarios, and selection of the optimal model form for specific regions or vegetation types, which is crucial for improved precision.

4.2. Impact and Change of Chilling

Temperature exerts a dual influence on spring phenology, that is, low temperatures are necessary to terminate endodormancy and the accumulation of heat is required for cessation of ecodormancy (Chuine et al., 2016). A

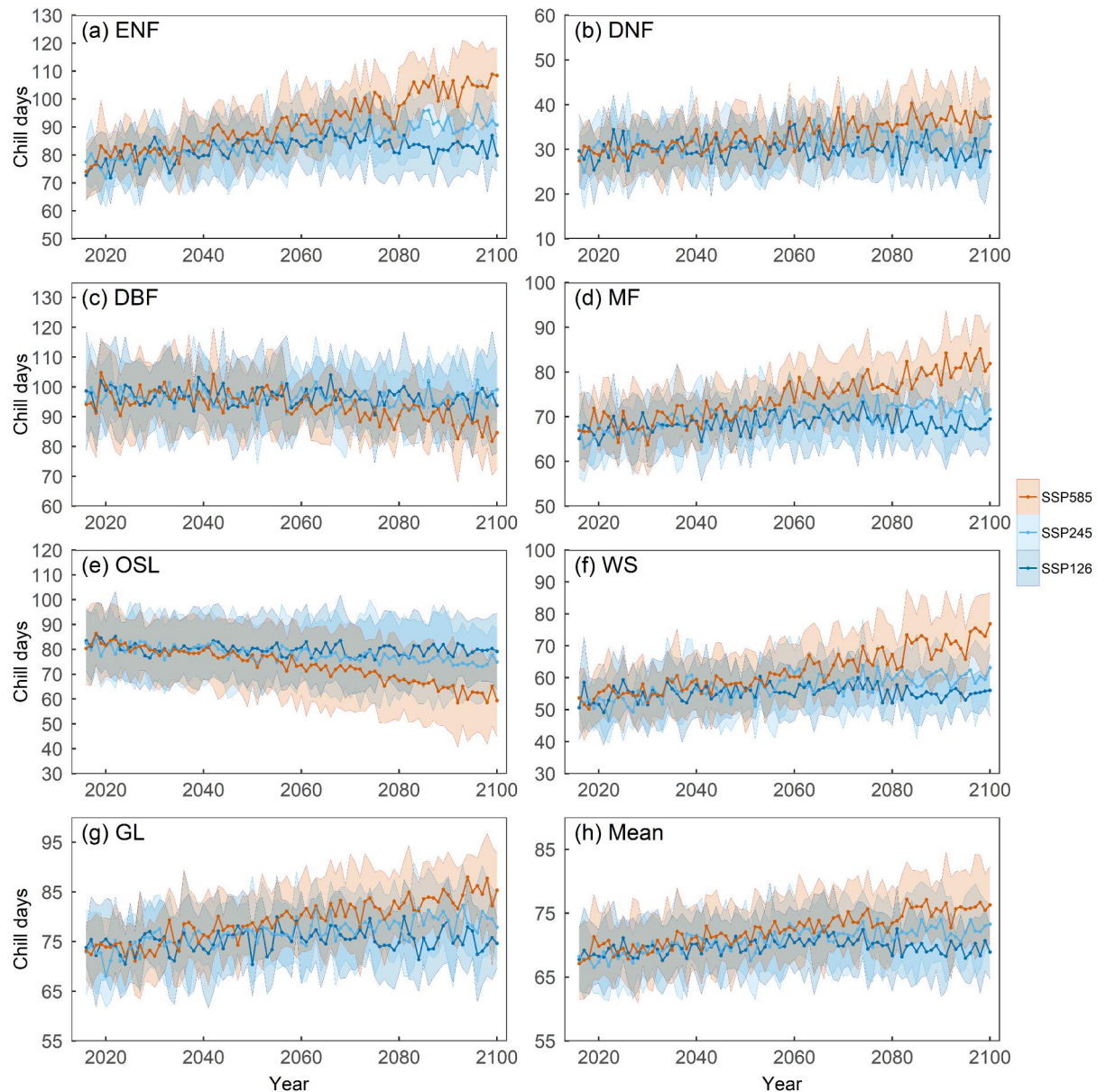


Figure 5. Temporal variation in the number of chill days under the three scenarios in the regions where the seven vegetation types are located: (a) evergreen needleleaf forest (ENF), (b) deciduous needleleaf forest (DNF), (c) deciduous broadleaf forest (DBF), (d) mixed forest (MF), (e) open shrubland (OSL), (f) woody savannah (WS), and (g) grassland (GL). (h) Temporal variation in mean chill days across the study area under the three scenarios. Shading represents one standard deviation of chill days calculated based on temperature data from the eight CMIP6 climate models under each scenario.

two-phase model considers the additional requirement of accumulated chilling compared with a one-phase model. The similar performance of the two types of models suggests that the requirement for chilling has already been met under current conditions. It is worth noting that there are differences in sensitivity to chilling accumulation and heat accumulation among different tree species. For example, the flowering date for chestnut trees in Beijing (China) is dominated by the heat accumulation rate, the leaf-unfolding time of walnut trees in Davis (California, USA) is mainly affected by the chilling accumulation rate, and the flowering time of cherry trees in Klein-Altendorf (Germany) is affected by both chilling accumulation and heat accumulation (Luedeling et al., 2013). Under the background of global warming, the spring phenology of tree species that are sensitive to heat accumulation might advance owing to faster heat accumulation, while the flowering or leaf-unfolding time of tree species that are sensitive to chilling accumulation might be delayed owing to insufficient chilling accumulation. However, some studies have shown that ongoing global warming might not necessarily reduce chilling

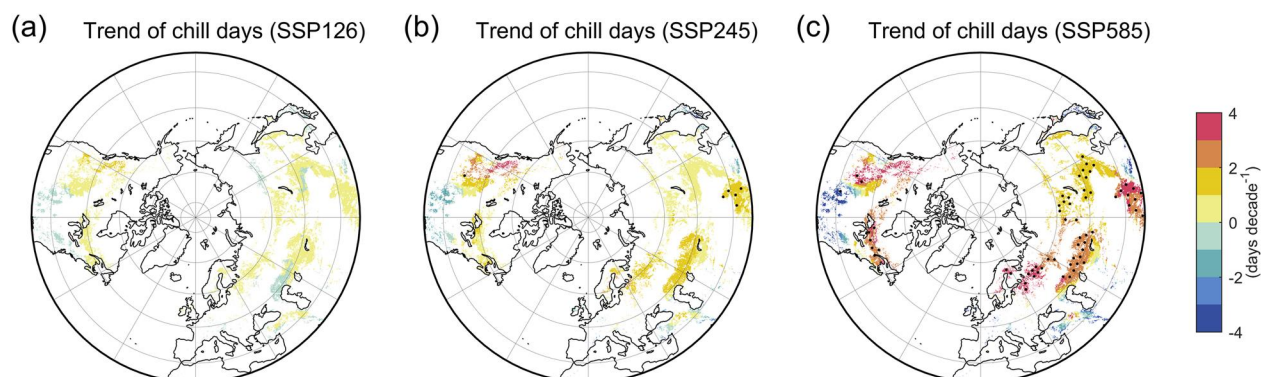


Figure 6. Spatial pattern of trend of chill days under the (a) SSP126, (c) SSP245, and (c) SSP585 scenarios. Dots represent regions with a statistically significant trend.

accumulation. For example, Juknys et al. (2016) noted that chilling at 55°N increased at a rate of 3.6 hr per year during 1920–2013. Our results showed that under the intense warming (i.e., the SSP585 scenario), the number of chill days gradually increased (except for DBF and OSL). This result might be because the average annual temperature of the areas where DBF and OSL are located is >10°C, and thus warming would cause reduction in the number of chill days. Conversely, the average annual temperature of the areas of the other vegetation types is <10°C, and for some it is even <0°C (i.e., DNF); thus, warming would increase the number of chill days. For GL, studies have shown that chilling accumulation is not an effective predictor of the vegetation green-up date. This inadequacy primarily arises because of the predominant influence of water limitation (i.e., precipitation and relative humidity) on vegetation phenology in such regions.

4.3. Changes in Future Phenology

Phenological patterns of vegetation in temperate and boreal regions are responsive to shifts in environmental factors, with pronounced emphasis on temperature variations. The advancement of spring phenology resulting from temperature increase has been extensively documented (Fu et al., 2015; Menzel et al., 2006; Peñuelas & Filella, 2001). Our research showed that spring phenology will advance with increasing temperature and will be delayed when temperature decreases. Previous phenology prediction studies were based mainly on different RCP scenarios. For the scenario of temperature increase (e.g., RCP 8.5), spring phenology mainly showed a trend of advance, although variation in the predicted advancement of phenology might reflect differences in study scale and models used (Asse et al., 2020; F. Meng et al., 2021; L. Meng et al., 2021; Wang et al., 2022; Zimmer et al., 2022). Under the optimistic climate change scenario (e.g., RCP 2.6), the temperatures of some regions might continue to increase, whereas the temperatures in other regions might gradually decrease (Liu et al., 2019). The spring phenology of vegetation primarily exhibits delay in response to decreasing temperatures (Jeong et al., 2013). Our findings indicated that spring phenology can track temperature changes, and as the temperature trends shift, the phenology trends also shift accordingly. Our results showed that under strong warming conditions, the phenology of all vegetation types will advance. This is because warming increases the number of chill days, thereby reducing the heat requirements, which are quickly satisfied and result in advancement of spring phenology. However, early phenology does not necessarily imply sustained greening because vegetation growth might be inhibited once temperatures exceed the optimal temperature range (Zhang et al., 2022). For the case of reduced chill days, advance in phenology might be due to the accumulation of heat caused by warming compensating for the increased heat demand caused by the reduction in chill days. In the case of moderate warming, the reversal of the trend of phenology advancement might reflect the increase in heat requirements caused by reduction in chill days.

4.4. Uncertainty

The models used in this study account for the influences of chilling, forcing, and the photoperiod on spring phenology; however, it should be noted that other environmental factors might also exert an impact. For example, it has been demonstrated that the effects of daytime and nighttime temperatures on spring phenology are asymmetrical and vary depending on vegetation type (Fu et al., 2016; Mo, Zhang, Jiang, et al., 2023; Mo, Zhang,

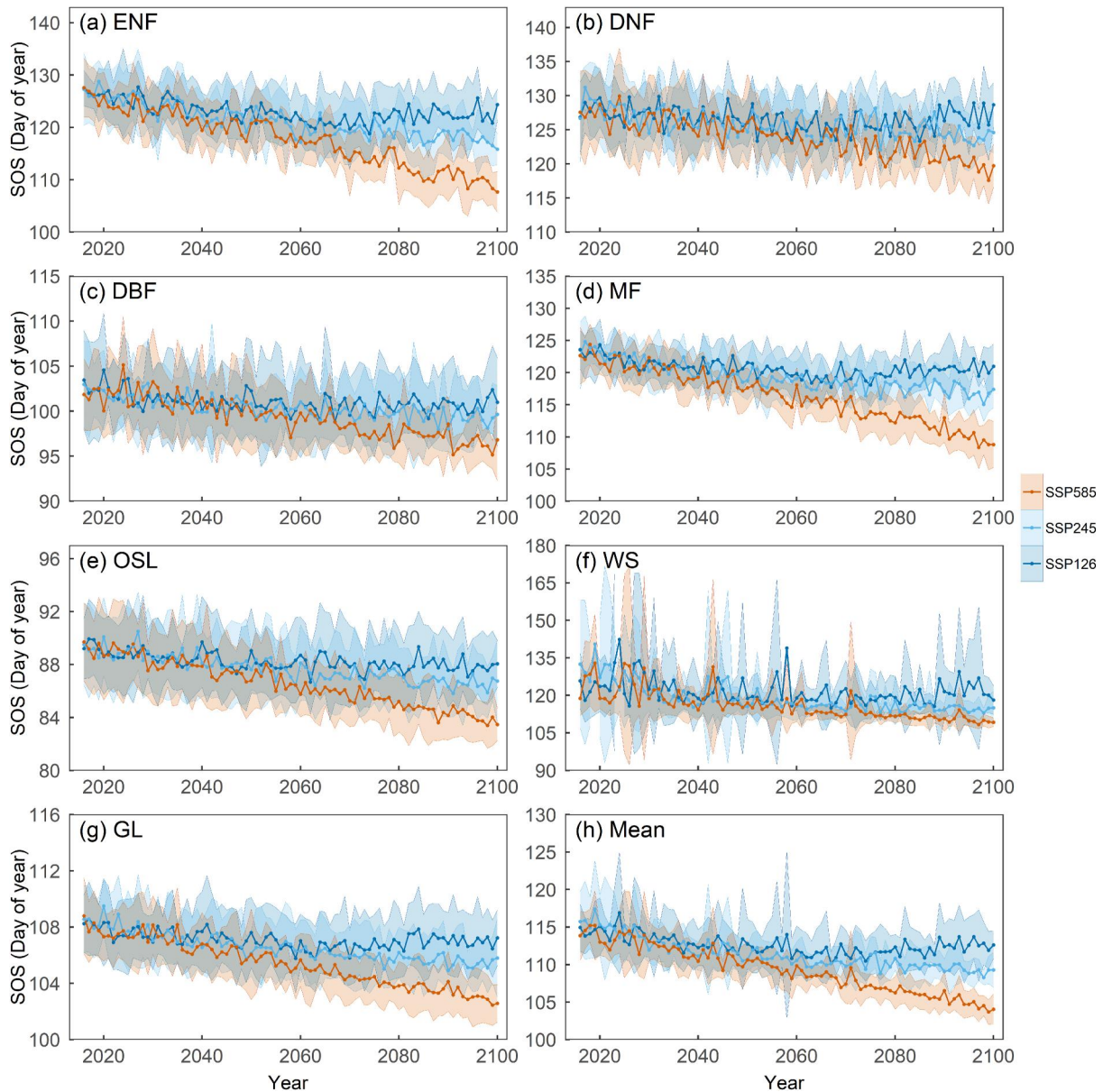


Figure 7. Temporal variation in the mean SOS of the seven vegetation types during 2021–2100 under the three warming scenarios: (a) evergreen needleleaf forest (ENF), (b) deciduous needleleaf forest (DNF), (c) deciduous broadleaf forest (DBF), (d) mixed forest (MF), (e) open shrubland (OSL), (f) woody savannah (WS), and (g) grassland (GL). (h) Temporal variation in the mean SOS across the study area under the three warming scenarios. Shading represents one standard deviation of the predicted SOS based on temperature data from the eight CMIP6 climate models under each scenario.

Liu, et al., 2023). Additionally, extreme weather events, especially frost, affect spring phenology (Mo, Zhang, Jiang, et al., 2023; Mo, Zhang, Liu, et al., 2023). Future spring phenology models should incorporate these new findings to better simulate phenological changes. With the rapid advancement of computer science in recent years, machine learning methods have also been applied to phenology prediction (Fu et al., 2022). Compared with process-based models, machine learning models lack theoretical interpretation; however, they can achieve higher simulation accuracy. In the future, a combination of process-based and machine learning models could be used to improve phenology prediction accuracy.

5. Conclusions

The performance of each of the 11 spring phenology models considered in this study was relatively close and better than that of the NULL model. The performance of the one-phase models was found comparable to that of

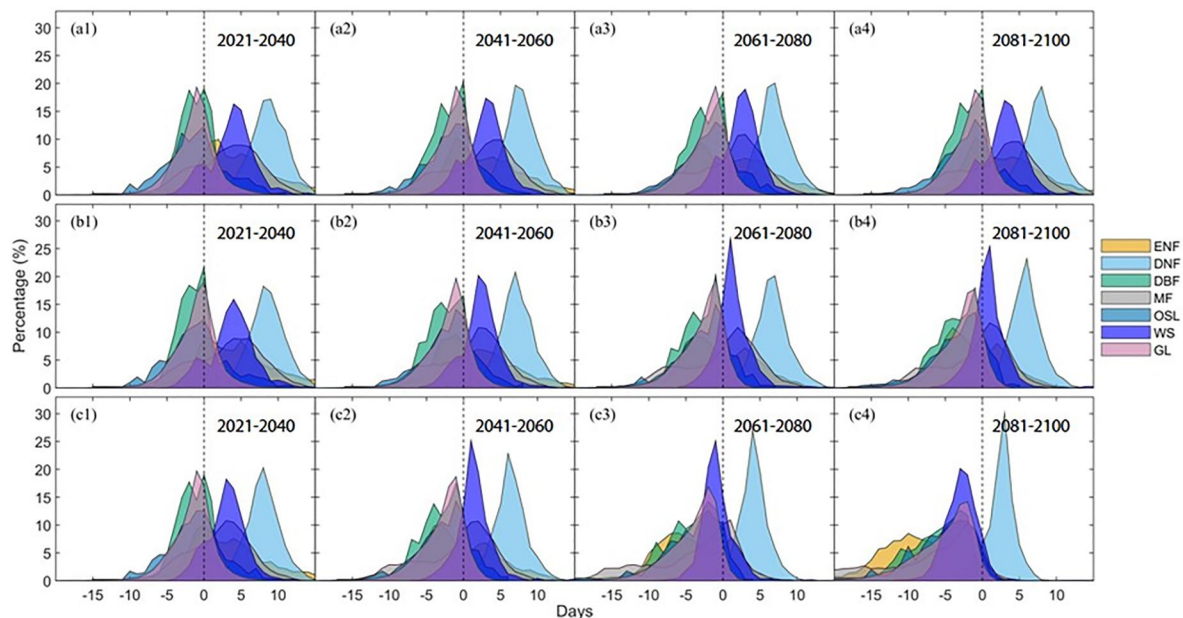


Figure 8. Changes in the mean SOS of the seven vegetation types in different periods under the three SSP scenarios. Histograms show the difference between the mean SOS of the seven vegetation types in the four future periods and the mean SOS of the historical period (1982–2015) under the (a1–a4) SSP126, (b1–b4) SSP245, and (c1–c4) SSP585 scenarios. All vertical lines are straight lines with SOS changes = 0 days. The seven vegetation types are evergreen needleleaf forest (ENF), deciduous needleleaf forest (DNF), deciduous broadleaf forest (DBF), mixed forest (MF), open shrubland (OSL), woody savannah (WS), and grassland (GL).

the two-phase models, although the best model varied depending on vegetation type. The simulated SOS of each model had a similar spatial pattern, with all models explaining >75% of the variation. Under the strong warming scenario (SSP585), spring phenology will continue to advance, whereas under the SSP126 scenario, the trend of advance in spring phenology will reverse by approximately 2060. The sustained trend of advance of the SOS might be related to the rapid fulfillment of forcing under strong warming conditions, whereas moderate warming might reduce chilling, which requires longer to compensate for the higher forcing requirement, thereby leading to a delay in the SOS. Our results indicated that under different warming conditions, phenological trends might exhibit different patterns, which could have broad impact on species interactions, biodiversity, and ecosystem function.

Conflict of Interest

The authors declare no conflicts of interest relevant to this study.

Data Availability Statement

Land cover data are available in Friedl et al. (2022). ERA-Interim data set is available in Li (2018). Climate scenarios data set can be found at <https://esgf-node.llnl.gov/search/cmip6/>. GIMMS NDVI data are available in The, N. (2018).

References

- Asse, D., Randin, C. F., Bonhomme, M., Delestrade, A., & Chuine, I. (2020). Process-based models outcompete correlative models in projecting spring phenology of trees in a future warmer climate. *Agricultural and Forest Meteorology*, 285, 107931. <https://doi.org/10.1016/j.agrformet.2020.107931>
- Basler, D. (2016). Evaluating phenological models for the prediction of leaf-out dates in six temperate tree species across central Europe. *Agricultural and Forest Meteorology*, 217, 10–21. <https://doi.org/10.1016/j.agrformet.2015.11.007>
- Berra, E. F., & Gaulton, R. (2021). Remote sensing of temperate and boreal forest phenology: A review of progress, challenges and opportunities in the intercomparison of in-situ and satellite phenological metrics. *Forest Ecology and Management*, 480, 118663. <https://doi.org/10.1016/j.foreco.2020.118663>
- Berrisford, P., Dee, D., Poli, P., Brugge, R., Fielding, K., Fuentes, M., et al. (2011). The ERA-interim archive: Version 2.0. *Nihon Seirigaku Zasshi Journal of the Physiological Society of Japan*, 31(10).

Acknowledgments

This study was funded by the National Science Fund for Distinguished Young Scholars (Grant 42025101), Funds for International Cooperation and Exchange of the National Natural Science Foundation of China (42261144755), Joint Fund for Regional Innovation and Development of the NSFC (U21A2039), Joint China–Sweden Mobility Program (Grant CH2020-8656), and 111 Project (B18006). We thank James Buxton for polishing the English text of a draft of this manuscript. We appreciate the reviewers' constructive comments and helpful suggestions.

- Berrisford, P., Dee, D. P., Fielding, K., Fuentes, M., Källberg, P. W., Kobayashi, S., & Uppala, S. M. (2009). *The ERA-interim archive*. Era Report.
- Blümel, K., & Chmielewski, F.-M. (2012). Shortcomings of classical phenological forcing models and a way to overcome them. *Agricultural and Forest Meteorology*, *164*, 10–19. <https://doi.org/10.1016/j.agrformet.2012.05.001>
- Cannell, M., & Smith, R. (1983). Thermal time, chill days and prediction of budburst in *Picea sitchensis*. *Journal of Applied Ecology*, *20*(3), 951–963. <https://doi.org/10.2307/2403139>
- Chen, A., Mao, J., Ricciuto, D., Lu, D., Xiao, J., Li, X., et al. (2021). Seasonal changes in GPP/SIF ratios and their climatic determinants across the Northern Hemisphere. *Global Change Biology*, *27*(20), 5186–5197. <https://doi.org/10.1111/gcb.15775>
- Chuine, I., Bonhomme, M., Legave, J. M., García de Cortázar-Atauri, I., Charrier, G., Lacombe, A., & Améglio, T. (2016). Can phenological models predict tree phenology accurately in the future? The unrevealed hurdle of endodormancy break. *Global Change Biology*, *22*(10), 3444–3460. <https://doi.org/10.1111/gcb.13383>
- Chuine, I., Cour, P., & Rousseau, D. (1999). Selecting models to predict the timing of flowering of temperate trees: Implications for tree phenology modelling. *Plant, Cell and Environment*, *22*(1), 1–13. <https://doi.org/10.1046/j.1365-3040.1999.00395.x>
- Cleland, E. E., Chuine, I., Menzel, A., Mooney, H. A., & Schwartz, M. D. (2007). Shifting plant phenology in response to global change. *Trends in Ecology & Evolution*, *22*(7), 357–365. <https://doi.org/10.1016/j.tree.2007.04.003>
- Cong, N., Wang, T., Nan, H., Ma, Y., Wang, X., Myneni, R. B., & Piao, S. (2013). Changes in satellite-derived spring vegetation green-up date and its linkage to climate in China from 1982 to 2010: A multimethod analysis. *Global Change Biology*, *19*(3), 881–891. <https://doi.org/10.1111/gcb.12077>
- Črepinšek, Z., Kajfež-Bogataj, L., & Bergant, K. (2006). Modelling of weather variability effect on fitophenology. *Ecological Modelling*, *194*(1–3), 256–265. <https://doi.org/10.1016/j.ecolmodel.2005.10.020>
- Eyring, V., Bony, S., Meehl, G. A., Senior, C. A., Stevens, B., Stouffer, R. J., & Taylor, K. E. (2016). Overview of the Coupled model inter-comparison project phase 6 (CMIP6) experimental design and organization. *Geoscientific Model Development*, *9*(5), 1937–1958. <https://doi.org/10.5194/gmd-9-1937-2016>
- Friedl, M., & Sulla-Menasse, D. (2022). MODIS/Terra+Aqua land cover type yearly L3 global 0.05Deg CMG V061 [Dataset]. NASA EOSDIS Land Processes Distributed Active Archive Center. <https://doi.org/10.5067/MODIS/MCD12C1.061>
- Fu, Y., Li, X., Zhou, X., Geng, X., Guo, Y., & Zhang, Y. (2020). Progress in plant phenology modeling under global climate change. *Science China Earth Sciences*, *63*(9), 1–11. <https://doi.org/10.1007/s11430-019-9622-2>
- Fu, Y. H., Li, X., Chen, S., Wu, Z., Su, J., Li, X., et al. (2022). Soil moisture regulates warming responses of autumn photosynthetic transition dates in subtropical forests. *Global Change Biology*, *28*(16), 4935–4946. <https://doi.org/10.1111/gcb.16227>
- Fu, Y. H., Liu, Y., De Boeck, H. J., Menzel, A., Nijs, I., Peaucelle, M., et al. (2016). Three times greater weight of daytime than of night-time temperature on leaf unfolding phenology in temperate trees. *New Phytologist*, *212*(3), 590–597. <https://doi.org/10.1111/nph.14073>
- Fu, Y. H., Piao, S., Zhou, X., Geng, X., Hao, F., Vitasse, Y., & Janssens, I. A. (2019). Short photoperiod reduces the temperature sensitivity of leaf-out in saplings of *Fagus sylvatica* but not in horse chestnut. *Global Change Biology*, *25*(5), 1696–1703. <https://doi.org/10.1111/gcb.14599>
- Fu, Y. H., Zhao, H., Piao, S., Peaucelle, M., Peng, S., Zhou, G., et al. (2015). Declining global warming effects on the phenology of spring leaf unfolding. *Nature*, *526*(7571), 104–107. <https://doi.org/10.1038/nature15402>
- Hänninen, H. (1990). Modelling bud dormancy release in trees from cool and temperate regions.
- Huang, M., Piao, S., Janssens, I. A., Zhu, Z., Wang, T., Wu, D., et al. (2017). Velocity of change in vegetation productivity over northern high latitudes. *Nature Ecology & Evolution*, *1*(11), 1649–1654. <https://doi.org/10.1038/s41559-017-0328-y>
- Hufkens, K., Basler, D., Milliman, T., Melaas, E. K., & Richardson, A. D. (2018). An integrated phenology modelling framework in R. *Methods in Ecology and Evolution*, *9*(5), 1276–1285. <https://doi.org/10.1111/2041-210x.12970>
- Hunter, A. F., & Lechowicz, M. J. (1992). Predicting the timing of budburst in temperate trees. *Journal of Applied Ecology*, *29*(3), 597–604. <https://doi.org/10.2307/2404467>
- Jakubauskas, M. E., Legates, D. R., & Kastens, J. H. (2001). Harmonic analysis of time-series AVHRR NDVI data. *Photogrammetric Engineering & Remote Sensing*, *67*(4), 461–470.
- Jeong, S. J., Ho, C. H., Gim, H. J., & Brown, M. E. (2011). Phenology shifts at start vs. end of growing season in temperate vegetation over the Northern Hemisphere for the period 1982–2008. *Global Change Biology*, *17*(7), 2385–2399. <https://doi.org/10.1111/j.1365-2486.2011.02397.x>
- Jeong, S. J., Medvigy, D., Shevliakova, E., & Malyshev, S. (2013). Predicting changes in temperate forest budburst using continental-scale observations and models. *Geophysical Research Letters*, *40*(2), 359–364. <https://doi.org/10.1029/2012gl054431>
- Jonsson, P., & Eklundh, L. (2002). Seasonality extraction by function fitting to time-series of satellite sensor data. *IEEE Transactions on Geoscience and Remote Sensing*, *40*(8), 1824–1832. <https://doi.org/10.1109/tgrs.2002.802519>
- Jonsson, P., & Eklundh, L. (2004). TIMESAT—A program for analyzing time-series of satellite sensor data. *Computers & Geosciences*, *30*(8), 833–845. <https://doi.org/10.1016/j.cageo.2004.05.006>
- Juknys, R., Kanapickas, A., Šveikauskaitė, I., & Sujetovienė, G. (2016). Response of deciduous trees spring phenology to recent and projected climate change in Central Lithuania. *International Journal of Biometeorology*, *60*(10), 1589–1602. <https://doi.org/10.1007/s00484-016-1149-4>
- Keenan, T. F., Gray, J., Friedl, M. A., Toomey, M., Bohrer, G., Hollinger, D. Y., et al. (2014). Net carbon uptake has increased through warming-induced changes in temperate forest phenology. *Nature Climate Change*, *4*(7), 598–604. <https://doi.org/10.1038/Nclimate2253>
- Kramer, K. (1994). Selecting a model to predict the onset of growth of *Fagus sylvatica*. *Journal of Applied Ecology*, *31*(1), 172–181. <https://doi.org/10.2307/2404609>
- Landsberg, J. (1974). Apple fruit bud development and growth; analysis and an empirical model. *Annals of Botany*, *38*(5), 1013–1023. <https://doi.org/10.1093/oxfordjournals.aob.a084891>
- Lang, G., Early, J. D., Martin, G., & Darnell, R. (1987). Endo-para-and ecodormancy: Physiological terminology and classification for dormancy research. *HortScience*, *22*(3), 371–377. <https://doi.org/10.21273/hortsci.22.5.701b>
- Li, C., Zwiers, F., Zhang, X., Li, G., Sun, Y., & Wehner, M. (2021). Changes in annual extremes of daily temperature and precipitation in CMIP6 models. *Journal of Climate*, *34*(9), 3441–3460. <https://doi.org/10.1175/jcli-d-19-1013.1>
- Li, F. (2018). Dataset of ERA-interim global surface air temperature reanalysis (1979–2016) [Dataset]. National Tibetan Plateau / Third Pole Environment Data Center. Retrieved from <https://data.tpdc.ac.cn/zh-hans/data/bd429368-b5f6-430b-a4bc-20cc489e832a/>
- Lieth, H. (1974). Purposes of a phenology book. In *Phenology and seasonality modeling* (pp. 3–19). Springer.
- Liu, Q., Fu, Y. H., Liu, Y., Janssens, I. A., & Piao, S. (2018). Simulating the onset of spring vegetation growth across the Northern Hemisphere. *Global Change Biology*, *24*(3), 1342–1356. <https://doi.org/10.1111/gcb.13954>
- Liu, Q., Piao, S., Fu, Y. H., Gao, M., Peñuelas, J., & Janssens, I. A. (2019). Climatic warming increases spatial synchrony in spring vegetation phenology across the Northern Hemisphere. *Geophysical Research Letters*, *46*(3), 1641–1650. <https://doi.org/10.1029/2018gl081370>

- Luedeling, E., Guo, L., Dai, J., Leslie, C., & Blanke, M. M. (2013). Differential responses of trees to temperature variation during the chilling and forcing phases. *Agricultural and Forest Meteorology*, *181*, 33–42. <https://doi.org/10.1016/j.agrformet.2013.06.018>
- Masle, J., Doussinault, G., Farquhar, G., & Sun, B. (1989). Foliar stage in wheat correlates better to photothermal time than to thermal time. *Plant, Cell and Environment*, *12*(3), 235–247. <https://doi.org/10.1111/j.1365-3040.1989.tb01938.x>
- Masson-Delmotte, V., Zhai, P., Pirani, A., Connors, S. L., Péan, C., Berger, S., et al. (2021). In *Climate change 2021: The physical science basis. Contribution of working group I to the sixth assessment report of the intergovernmental panel on climate change*. IPCC.
- Meinshausen, M., Nicholls, Z. R., Lewis, J., Gidden, M. J., Vogel, E., Freund, M., et al. (2020). The shared socio-economic pathway (SSP) greenhouse gas concentrations and their extensions to 2500. *Geoscientific Model Development*, *13*(8), 3571–3605. <https://doi.org/10.5194/gmd-13-3571-2020>
- Meng, F., Huang, L., Chen, A., Zhang, Y., & Piao, S. (2021). Spring and autumn phenology across the Tibetan Plateau inferred from normalized difference vegetation index and solar-induced chlorophyll fluorescence. *Big Earth Data*, *5*(2), 182–200. <https://doi.org/10.1080/20964471.2021.1920661>
- Meng, L., Zhou, Y., Gu, L., Richardson, A. D., Peñuelas, J., Fu, Y., et al. (2021). Photoperiod decelerates the advance of spring phenology of six deciduous tree species under climate warming. *Global Change Biology*, *27*(12), 2914–2927. <https://doi.org/10.1111/gcb.15575>
- Menzel, A. (2002). Phenology: Its importance to the global change community. *Climatic Change*, *54*(4), 379–385. <https://doi.org/10.1023/a:1016125215496>
- Menzel, A., Sparks, T. H., Estrella, N., Koch, E., Aasa, A., Ahas, R., et al. (2006). European phenological response to climate change matches the warming pattern. *Global Change Biology*, *12*(10), 1969–1976. <https://doi.org/10.1111/j.1365-2486.2006.01193.x>
- Mo, Y., Chen, S., Jin, J., Lu, X., & Jiang, H. (2019). Temporal and spatial dynamics of phenology along the North–South Transect of Northeast Asia. *International Journal of Remote Sensing*, *40*(20), 7922–7940. <https://doi.org/10.1080/01431161.2019.1608390>
- Mo, Y., Zhang, J., Jiang, H., & Fu, Y. (2023). A comparative study of 17 phenological models to predict the start of the growing season. *Frontiers in Forests and Global Change*, *5*, 276. <https://doi.org/10.3389/ffgc.2022.1032066>
- Mo, Y., Zhang, X., Liu, Z., Zhang, J., Hao, F., & Fu, Y. (2023). Effects of climate extremes on spring phenology of temperate vegetation in China. *Remote Sensing*, *15*(3), 686. <https://doi.org/10.3390/rs15030686>
- Morales, M. A., Dodge, G. J., & Inouye, D. W. (2005). A phenological mid-domain effect in flowering diversity. *Oecologia*, *142*(1), 83–89. <https://doi.org/10.1007/s00442-004-1694-0>
- Murray, M., Cannell, M., & Smith, R. (1989). Date of budburst of fifteen tree species in Britain following climatic warming. *Journal of Applied Ecology*, *26*(2), 693–700. <https://doi.org/10.2307/2404093>
- O'Neill, B. C., Tebaldi, C., Vuuren, D. P. v., Eyring, V., Friedlingstein, P., Hurtt, G., et al. (2016). The scenario model intercomparison project (ScenarioMIP) for CMIP6. *Geoscientific Model Development*, *9*(9), 3461–3482. <https://doi.org/10.5194/gmd-9-3461-2016>
- Pau, S., Wolkovich, E. M., Cook, B. I., Davies, T. J., Kraft, N. J., Bolmgren, K., et al. (2011). Predicting phenology by integrating ecology, evolution and climate science. *Global Change Biology*, *17*(12), 3633–3643. <https://doi.org/10.1111/j.1365-2486.2011.02515.x>
- Peñuelas, J., & Filella, I. (2001). Responses to a warming world. *Science*, *294*(5543), 793–795. <https://doi.org/10.1126/science.1066860>
- Piao, S., Fang, J., Zhou, L., Ciais, P., & Zhu, B. (2006). Variations in satellite-derived phenology in China's temperate vegetation. *Global Change Biology*, *12*(4), 672–685. <https://doi.org/10.1111/j.1365-2486.2006.01123.x>
- Piao, S., Liu, Q., Chen, A., Janssens, I. A., Fu, Y., Dai, J., et al. (2019). Plant phenology and global climate change: Current progresses and challenges. *Global Change Biology*, *25*(6), 1922–1940. <https://doi.org/10.1111/gcb.14619>
- Piao, S., Wang, X., Park, T., Chen, C., Lian, X., He, Y., et al. (2020). Characteristics, drivers and feedbacks of global greening. *Nature Reviews Earth & Environment*, *1*(1), 14–27. <https://doi.org/10.1038/s43017-019-0001-x>
- Pinzon, J., & Tucker, C. (2014). A Non-Stationary 1981–2012 AVHRR NDVI3g time series. *Remote Sensing*, *6*(8), 6929–6960. <https://doi.org/10.3390/rs6086929>
- Reaumur, R. D. (1735). Observations du thermomètre faites à Paris pendant l'année 1735, comparées avec celles qui ont été faites sous la ligne, à l'Isle de France, à Alger et quelques unes de nos îles de l'Amérique. *Mémoires l'Académie R des Sci*, 545–576.
- Reed, B. C., Schwartz, M. D., & Xiao, X. (2009). Remote sensing phenology. In *Phenology of ecosystem processes* (pp. 231–246). Springer.
- Roerink, G. J., Menenti, M., & Verhoef, W. (2000). Reconstructing cloudfree NDVI composites using Fourier analysis of time series. *International Journal of Remote Sensing*, *21*(9), 1911–1917. <https://doi.org/10.1080/014311600209814>
- Solomon, S. (2007). IPCC (2007): Climate change the physical science basis. In *Paper presented at the Agu fall meeting abstracts*.
- Stocker, T. (2014). In *Climate change 2013: The physical science basis: Working group I contribution to the fifth assessment report of the intergovernmental panel on climate change*. Cambridge university press.
- The, N. (2018). Global GIMMS NDVI3g v1 dataset (1981–2015) [Dataset]. National Tibetan Plateau / Third Pole Environment Data Center. Retrieved from <https://data.tpdc.ac.cn/en/data/9775f2b4-7370-4e5e-a537-3482c9a83d88/>
- Vitasse, Y., François, C., Delpierre, N., Dufréne, E., Kremer, A., Chuine, I., & Delzon, S. (2011). Assessing the effects of climate change on the phenology of European temperate trees. *Agricultural and Forest Meteorology*, *151*(7), 969–980. <https://doi.org/10.1016/j.agrformet.2011.03.003>
- Wang, H., Lin, S., Dai, J., & Ge, Q. (2022). Modeling the effect of adaptation to future climate change on spring phenological trend of European beech (*Fagus sylvatica* L.). *Science of the Total Environment*, *846*, 157540. <https://doi.org/10.1016/j.scitotenv.2022.157540>
- Wang, J. Y. (1960). A critique of the heat unit approach to plant response studies. *Ecology*, *41*(4), 785–790. <https://doi.org/10.2307/1931815>
- White, M. A., de Beurs, K. M., Didan, K., Inouye, D. W., Richardson, A. D., Jensen, O. P., et al. (2009). Intercomparison, interpretation, and assessment of spring phenology in North America estimated from remote sensing for 1982–2006. *Global Change Biology*, *15*(10), 2335–2359. <https://doi.org/10.1111/j.1365-2486.2009.01910.x>
- Wolkovich, E. M., Cook, B. I., & Davies, T. J. (2014). Progress towards an interdisciplinary science of plant phenology: Building predictions across space, time and species diversity. *New Phytologist*, *201*(4), 1156–1162. <https://doi.org/10.1111/nph.12599>
- Wu, W.-B., Peng, Y., Tang, H.-J., Zhou, Q.-B., Chen, Z.-X., & Shibasaki, R. (2010). Characterizing spatial patterns of phenology in cropland of China based on remotely sensed data. *Agricultural Sciences in China*, *9*(1), 101–112. [https://doi.org/10.1016/s1671-2927\(09\)60073-0](https://doi.org/10.1016/s1671-2927(09)60073-0)
- Xiang, Y., Gubian, S., Suomela, B., & Hoeng, J. (2013). Generalized simulated annealing for global optimization: The GenSA package. *R J*, *5*(1), 13. <https://doi.org/10.32614/rj-2013-002>
- Yu, H., Luedeling, E., & Xu, J. (2010). Winter and spring warming result in delayed spring phenology on the Tibetan Plateau. *Proceedings of the National Academy of Sciences of the United States of America*, *107*(51), 22151–22156. <https://doi.org/10.1073/pnas.1012490107>
- Zeng, L., Wardlow, B. D., Xiang, D., Hu, S., & Li, D. (2020). A review of vegetation phenological metrics extraction using time-series, multispectral satellite data. *Remote Sensing of Environment*, *237*, 111511. <https://doi.org/10.1016/j.rse.2019.111511>
- Zhang, Y., Piao, S., Sun, Y., Rogers, B. M., Li, X., Lian, X., et al. (2022). Future reversal of warming-enhanced vegetation productivity in the Northern Hemisphere. *Nature Climate Change*, *12*(6), 581–586. <https://doi.org/10.1038/s41558-022-01374-w>

- Zhao, H., Fu, Y. H., Wang, X., Zhang, Y., Liu, Y., & Janssens, I. A. (2021). Diverging models introduce large uncertainty in future climate warming impact on spring phenology of temperate deciduous trees. *Science of the Total Environment*, 757, 143903. <https://doi.org/10.1016/j.scitotenv.2020.143903>
- Zimmer, S. N., Reeves, M. C., St. Peter, J. R., & Hanberry, B. B. (2022). Earlier green-up and senescence of temperate United States rangelands under future climate. *Modeling Earth Systems and Environment*, 8(4), 5389–5405. <https://doi.org/10.1007/s40808-022-01389-4>